CD34+ UCB stem cells attenuate TGF-**β** signaling and inhibit liver fibrosis: A new avenue for liver cirrhosis-carcinogenesis prevention

Wahyunia Likhayati Septiana
Department of Histology, Faculty of Medicine, Universitas Indonesia, Jakarta 10430, Indonesia, wahyunia179@gmail.com

Radiana Dhewayani Antarianto
Department of Histology, Faculty of Medicine, Universitas Indonesia, Jakarta 10430, Indonesia, radiana.dhewayani@ui.ac.id

Melva Louisa
Department of Pharmacology, Faculty of Medicine, Universitas Indonesia, Jakarta 10430, Indonesia, melva.louisa@gmail.com

Ahmad Aulia Jusuf
Department of Histology, Faculty of Medicine, Universitas Indonesia, Jakarta 10430, Indonesia, aljuswin04@yahoo.com

Atikah Chalida Barasila
Department of Histology, Faculty of Medicine, Universitas Indonesia, Jakarta 10430, Indonesia, ac.barasila@gmail.com

CD34+ UCB stem cells attenuate TGF-β signaling and inhibit liver fibrosis: A new avenue for liver cirrhosis-carcinogenesis prevention

Authors

Wahyunia Likhayati Septiana, Radiana Dhewayani Antarianto, Melva Louisa, Ahmad Aulia Jusuf, Atikah Chalida Barasila, Jeanne Adiwinata Pawitan, and Iqbal Fasha

CD34+ UCB stem cells attenuate TGF-β signaling and inhibit liver fibrosis: A new avenue for liver cirrhosis-carcinogenesis prevention

Wahyunia Likhayati Septiana[1], Radiana Dhewayani Antarianto[1,2*], Melva Louisa[3], Ahmad Aulia Jusuf[1,2], Atikah Chalida Barasila[1], Jeanne Adiwinata Pawitan[1,2], Iqbal Fasha[4]

[1]Department of Histology, Faculty of Medicine, Universitas Indonesia, Jakarta 10430, Indonesia
[2]Stem Cell and Tissue Engineering Research Cluster, Indonesian Medical Education and Research Institute (IMERI), Universitas Indonesia, Jakarta 10430, Indonesia
[3]Department of Pharmacology, Faculty of Medicine, Universitas Indonesia, Jakarta 10430, Indonesia
[4]Department of Biology, Faculty of Medicine, Universitas Indonesia, Jakarta 10430, Indonesia

*E-mail: radiana.dhewayani@ui.ac.id

Abstract

Background: The liver microenvironment plays a key role in liver fibrosis and carcinogenesis. This study aimed to fill the gap in knowledge on the interaction between hepatic stellate cells and endothelial progenitor cells with biomarkers of liver fibrosis and/or carcinogenesis, including Col1A1, TGF-β, and tenascin-C. **Methods**: CD34+ stem cells were isolated from umbilical-cord-blood mononuclear cells. 2D and 3D co-culture of CD34+ UCB SCs and LX2 was performed. The cells were incubated in a CO_2 incubator for three days. Morphological observation, qRT-PCR of TGF-β1 and COL1A1, and immunocytochemistry of tenascin-C were performed. **Results**: CD34+ UCB SCs were viable in the 2D and 3D co-culture for 24 h. 3D co-culture of CD34+ UCB SCs and LX2 inhibited in vitro liver fibrosis by lowering Col 1A1 expression as compared to control. We observed lower TGF-β expression in 3D co-culture on days 1 and 2 followed by higher expression of TGF-β on day 3. 2D co-culture of CD34+ UCB SCs and LX2 showed a different level of COL1A1 and TGF- β expression compared with 3D co-culture. Spheroids from 2D co-culture of CD34+ UCB SCs and LX-2 showed immunoreactivity against tenascin-C. **Conclusion**: Interaction between LX-2 and CD34+ UCB SCs in 3D co-culture inhibits in vitro liver fibrosis. The viability of CD34+ UCB SCs is essential for attenuation of TGF-β signaling in LX-2.

Keywords: CD34+, collagen 1A1, spheroid formation, tenascin-C, TGF-β signaling, umbilical cord blood

Introduction

Hepatocellular carcinoma (HCC) causes 810,000 cancer mortalities each year.[1] The increasing number of hepatitis B virus (HBV) infection cases has led to a higher incidence of liver cancer in the developing world. It is estimated that 248 million people worldwide are infected with HBV.[2] According to Globocan 2018 data, the incidence rate of HCC in Indonesia was 5.8–8.4 per 100,000 people.[1] The risk of developing liver cancer in patients with HBV-induced cirrhosis is eight-fold higher than in HBV carriers without cirrhosis.[3]

At the heart of progression from HBV-induced cirrhosis to liver cancer is the liver microenvironment. The microenvironment of the liver comprises liver parenchymal cells (hepatocytes); non-parenchymal cells of the liver, e.g. kupfer cells, hepatic stellate cells, endothelial cells, and cholangiocytes; and the extracellular matrix (ECM). Interaction between cell-to-cell and cell-to-matrix in the liver microenvironment determines

tissue changes. Liver fibrosis, cirrhosis, and carcinogenesis occur as a spectrum of reversible to irreversible changes in liver histology. In vitro 3D co-culture of liver cells with or without non-liver cells offer a 3D liver microenvironment with cell-to-cell spatial contact and cell-to-matrix interactions, thus mimicking tissue responses. This method is useful for the study of liver fibrogenesis and carcinogenesis in the absence of culture plate attachment inherent in 2D co-culture. 2D co-culture potentially leads to biases from attached cells as they produce cell-adhesion molecules to the culture plate or each other. Cell-to-cell spatial contact and cell-to-matrix interaction in 2D co-culture is different from in vivo tissue response.[4–6]

Hepatic stellate-cell line LX-2 has been used as an established in vitro model of liver fibrosis or carcinogenesis. The characteristics of LX-2 are activated hepatic stellate cells with a myofibroblast phenotype, high proliferation abilities, more abundant collagen type I secretion to the ECM, and fewer matrix

metalloproteinase degradation enzymes. These characteristics support the progression of liver fibrosis into liver cirrhosis.[7,8] The main cytokine in the event of liver fibrosis and carcinogenesis is TGF-β.[3] TGF-β signaling also occurs at the initiation of HCC and the EMT process (metastasis of HCC). Co-culture of HCC with hepatic stellate cells produced a higher proliferation rate of HCC.[9] Hepatic stellate cells differentiate into cancer-associated fibroblasts (CAF) upon stimulation of the exosome or miRNA-21 secretion by HCCs in the microenvironment.[10] Cystein-rich 61 (CCN1/Cyr61) is an ECM protein that affects and increases the effect of the LX-2 cell line on Hep2G (liver cancer cell line) by promoting the viability, migration, and invasion capacity of Hep2G in vitro.[11]

The role of CD34^{+} hematopoietic SCs in liver cirrhosis and carcinogenesis is partially understood. CD34^{+} hematopoietic SCs are derived from the bone marrow by aspiration or from UCB.[12] The potency of CD34^{+} UCB SCs for liver regenerative therapy has been reported in in vivo studies. The use of CD34^{+} UCB SCs in non-obese, diabetic, and immunodeficient mice with liver injury demonstrated the fusion of the CD34^{+} UCB SCs with the liver tissue, improved liver parameters, and a reduced mortality rate in the mice.[12] CD34^{+} stem cells are also known as endothelial progenitor cells (EPCs). Patients with liver cirrhosis have an increased number of circulating EPCs, which correlates with the degree of liver cirrhosis. EPC can promote angiogenesis by secretion of VEGF and differentiation into mature endothelial cells followed by incorporation into injured vessels.[13–15] An in vitro study by Liu *et al.* demonstrated the release of placental growth factor (PlGF) from CAF which originated from activated hepatic stellate cells that increased angiogenesis in HCC.[16]

Fragmented concepts on the role of hepatic stellate cells and EPC from HCC patients, cirrhosis patients, liver fibrosis, and cancer animal models required further investigation into the interaction between hepatic stellate cells and EPCs at an in vitro level. This study aimed to fill the gap of knowledge on the interaction between hepatic stellate cells and EPCs with biomarkers of liver fibrosis and the carcinogenesis microenvironment, including Col1A1, TGF-β, and tenascin-C.

Methods

This study was an in vitro experimental study using two cell populations: CD34^{+} UCB SCs, which were isolated from the mononuclear fraction of UCB, and LX-2 cells, which were obtained from Millipore (Cat No. #SCC064). The experiments were replicated three times. This study was performed from August 2015 to September 2016 at the Institute of Human Virology and Cancer Biology Faculty of Medicine Universitas Indonesia–Cipto Mangunkusumo Central Hospital

(FKUI-RSCM), Department of Histology FKUI, the flow cytometry facility at the FKUI Integrated Lab, and the Stem Cell Medical Technology Integrated Service Unit at FKUI-RSCM. The protocol of this study was approved by the FKUI Ethical Committee (no 751a/UN2.F1/ETIK/VIII/2015).

Isolation and characterization of CD34^{+} UCB SCs. CD34^{+} UCB SCs were isolated from cryopreserved cord blood, which was a generous gift from Cellsafe and the Stem Cell Medical Technology Integrated Service Unit at RSCM-FKUI. After thawing the cryopreserved cord blood, the cells underwent erythrocyte lysis and were further separated by Ficoll-Hypaque gradient-density centrifugation. CD34^{+} cell isolation was performed using a human CD34 microbead kit (Miltenyi Biotec, Bergisch Gladbach, Germany) according to the manufacturer's instructions. The phenotype of UCB CD34^{+} SCs was evaluated by flow cytometry analysis of CD34.

2D co-culture of CD34^{+} UCB SCs and LX-2 cells. The co-culture process for CD34^{+} UCB SCs and LX-2 cells, in particular the maintenance of cell health, is difficult, so this study was only conducted over a period of three days. The 2D culture was performed using a 96-well plate with a total of 10,000 CD34^{+} UCB SCs per well in suspension with 10,000 LX-2 cells per well. Two wells of the 2D co-culture in the 96-well plate were prepared. The first well was observed under an inverted microscope, documented, and harvested after one day in culture. The second well underwent a similar protocol after two days in culture. In addition, a 2D culture was performed using a 24-well plate for the co-culture of CD34^{+} UCB SCs and LX-2 cells for three days. A total of 25,000 CD34^{+} UCB SCs per well were mixed with 25,000 LX-2 cells in suspension. The well was observed under an inverted microscope, documented, and harvested on day 3.

3D co-culture of CD34^{+} UCB SCs and LX-2 cells with the hanging drop method. This culture method used a 10 cm petri dish. One milliliter of a suspension comprised of 50,000 CD34+ and 50,000 LX-2 cells in a 1:1 (v/v) ratio was prepared. Furthermore, 30 µL of the suspension was carefully pipetted onto the inner side of a petri dish lid (open position). Each lid ultimately contained an average of 20–30 drops. The lower petri dish was filled with 5 mL of DMEM or PBS. In a single movement, the upper lid was flipped to obtain a closed petri dish position. The drops were hanging on the inner surface of the upper lid. The dish was incubated in a CO_2 incubator at 37 °C, 5% CO_2, and 95% humidity. Four dishes were prepared. Three dishes were harvested on each of day 1, day 2, and day 3. A fourth dish was used as a negative control and contained the 3D hanging drop monoculture of HSCs that were harvested on day 3.

A Quantitative reverse transcriptase PCR (qRT-PCR) of collagen 1 subtype A1 (COL1A1) and TGF-β1. RNA from the harvested cells was isolated using the TriPure RNA Isolation Reagent (Roche, France). cDNA synthesis from RNA samples was performed using AccuPower CycleScript RT PreMix (dN6) (Bioneer, US). qRT-PCR was used to measure the mRNA expression levels of COL1A1 and TGF-β1 and was performed with a LightCycler Nano Master (Roche, France) and these levels were compared to those of the housekeeping gene beta-actin. The forward primer used for COL1A1 was 5'AGGTCCCCCTGGAAAGAA-3', and the reverse primer for COL1A1 was 5'AATCCTCGAGCACCCTGA-3'; the forward primer for TGF-β1 was 5'TGAACCGGCCTTTCCTGCTTCTC ATG-3', and the reverse primer for TGF-β1 was 5'GCGGAAGTCAATGTACAGCTGCCGC-3'. The volume of the reagent was 20 μL, which comprised 3 μL PCR grade H_2O, 1 μL forward primer (10 μM), 1 μL reverse primer (10 μM), 10 μL SYBR-Green qRT-PCR Master Mix, and 5 μL (100 ng) cDNA template. The reagents were pipetted into LightCycler 8-Tube Strips (clear) (Roche, France). Then, they underwent LightCycler Nano Master qPCR with an optimized cycle protocol. The qRT-PCR result was obtained by calculation with Livak formulas.

Immunochemistry of tenascin-C. The harvested 2D and 3D co-cultures and the negative control were collected on day 3. The cells were fixed in methanol for 1 h. Nonspecific binding reduction with 10% donkey serum blocking solution was performed for 1 h. Incubation with anti-tenascin-C primary antibody sc9871 (Santa Cruz Biotechnology, US) was performed for 1 h in a moist chamber at room temperature. Incubation with biotinylated secondary antibody was performed, followed by streptavidin-conjugated peroxidase and 3,3'-diaminobenzidine (DAB) substrate addition. Nuclear counterstaining was performed with Hematoxylin Harris. The results were observed under an inverted microscope and documented. Areas of dark brown signals, which indicate positive tenascin-C expression, were described.

Statistical analysis. Data of qRT-PCR Col1A1 and TGF-β were entered into GraphPad Prism 8 software. Homogeneity or normal distribution of the data was tested with a Shapiro–Wilk test. The result was displayed as mean±SD for normal data distribution otherwise displayed as min, max, and median value. Further statistical analysis was conducted to test for differences between 2D and 3D co-culture.

Results

Characterization of CD34+ UCB SCs. The 2D culture of UCB SCs showed homogenous mononuclear cells with a round morphology, non-adherence to the well,

and suspension in the culture medium. Flow cytometry analysis revealed the mononuclear cell fraction to be the target population (Figure 1A). The isotype control is shown in Figure 1B. Flow cytometry analysis of MACS (magnetic-activated cell sorting) isolated CD34+ UCB SCs showed that the purity of CD34+ was 80%. This percentage was acquired from a gated population in Q4 (i.e. the right lower quadrant) (Figure 1C).

Morphology observation of 2D and 3D co-culture CD34+ UCB SCs and LX-2. Day 1 of 2D co-culture CD34+ UCB SCs and LX-2 showed the morphology of the LX-2 monolayer and suspended CD34+ UCB SCs on top of the single layer (Figure 2A), and 3D co-culture showed small cells aggregates of LX-2 and single round CD34+ UCB SCs suspended around the small cell aggregates (Figure 2E). Day 2 of 2D co-culture showed retraction in the periphery of the LX-2 monolayer and hardly any visible CD34+ UCB SCs (Figure 2B), and 3D co-culture showed medium-sized spheroids and the absence of CD34+ UCB-SC morphology outside the spheroid (Figure 2F). This result demonstrated that after two days of in vitro co-culture, CD34+ UCB SCs no longer present in the co-culture. Day 3 of 2D culture showed spheroid micromass formation of LX-2 in comparison with the monolayer of LX-2 monoculture (Figure 2C vs. Figure 2D), whereas 3D culture showed smaller spheroids in comparison to LX-2 3D monoculture (Figure 2G vs Figure 2H).

mRNA expression of COL1A1. qRT-PCR of COL1A1 mRNA expression level from the 2D co-culture of CD34+ UCB SCs and LX-2 cells, when normalized with control (monoculture of LX-2), showed a mean±SD COL1A1 expression level of 0.052±0.014 on day 1, 0.00003 on day 2, and 1.638±0.0003 on day 3 (Figure 3).

qRT-PCR of COL1A1 mRNA expression level from the 3D (hanging drop) co-culture of CD34+ UCB SCs and LX-2 cells, when normalized with the monoculture of LX-2 cells (control), showed a mean±SD COL1A1 expression level of 0.0075 on day 1, 0.0949±0.102 on day 2, and 0.6391±0.5689 on day 3 (Figure 3).

The data of Col1A1 expression is homogenous based on the Shapiro–Wilk test ($p = 0.053$, not significant). Comparative analysis using multiple t-tests between 2D and 3D co-culture on each day data set showed no statistically significant difference between each group ($p > 0.05$).

TGF-β1 mRNA expression. qRT-PCR of the TGF-β mRNA expression level from the 2D co-culture of CD34+ UCB SCs and LX-2 cells, when normalized with TGF-β expression of control, showed that min, max, and median expression level of TGF-β on day 1 was 46.0778, 83.142, and 64.049, respectively. On day 2, the

min, max, and median expression levels of TGF-β were 0.0154, 0.0442, and 0.0298, respectively. On day 3, the min, max, and median expression levels of TGF-βwere 0.091, 0.526, and 0.308, respectively (Figure 4).

qRT-PCR of the TGF-β mRNA expression level from the 3D (hanging drop) co-culture of CD34^{+} UCB SCs and LX-2 cells, when normalized with TGF-β expression of control, showed a min, max, and median expression level of TGF-β on day 1 of 0.01, 0.108, and 0.059, respectively. On day 2, the min, max, and median expression levels of TGF-β were 0.0665, 0.093, and 0.08, respectively. On day 3, the min, max, and median expression levels of TGF-β were 0.0348, 1.675, and 0.855, respectively (Figure 4).

Data of TGF-β expression was not distributed normally based on a Shapiro–Wilk test ($p = 0.007$, significant difference between each group data set). Comparative analysis using a non-parametric Wilcoxon rank test showed no statistically significant differences between each group ($p > 0.05$).
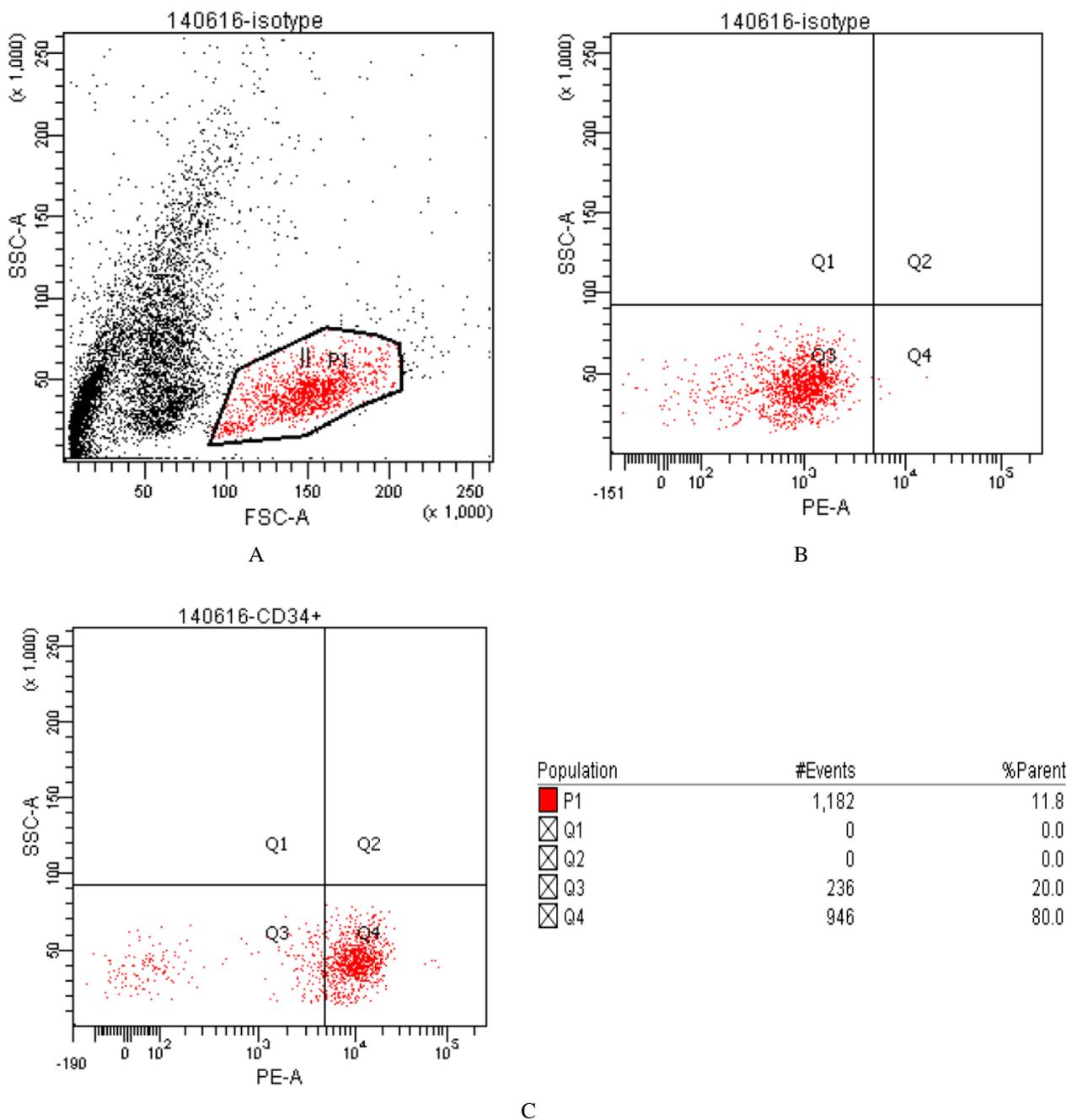

Population	#Events	%Parent
P1	1,182	11.8
Q1	0	0.0
Q2	0	0.0
Q3	236	20.0
Q4	946	80.0

Figure 1. Flow cytometry analysis from UCB SCs (A) Gating population (B) Isotype IgGγ1 (C) Flow cytometry analysis CD34^{+} MACS isolated UCB SCs
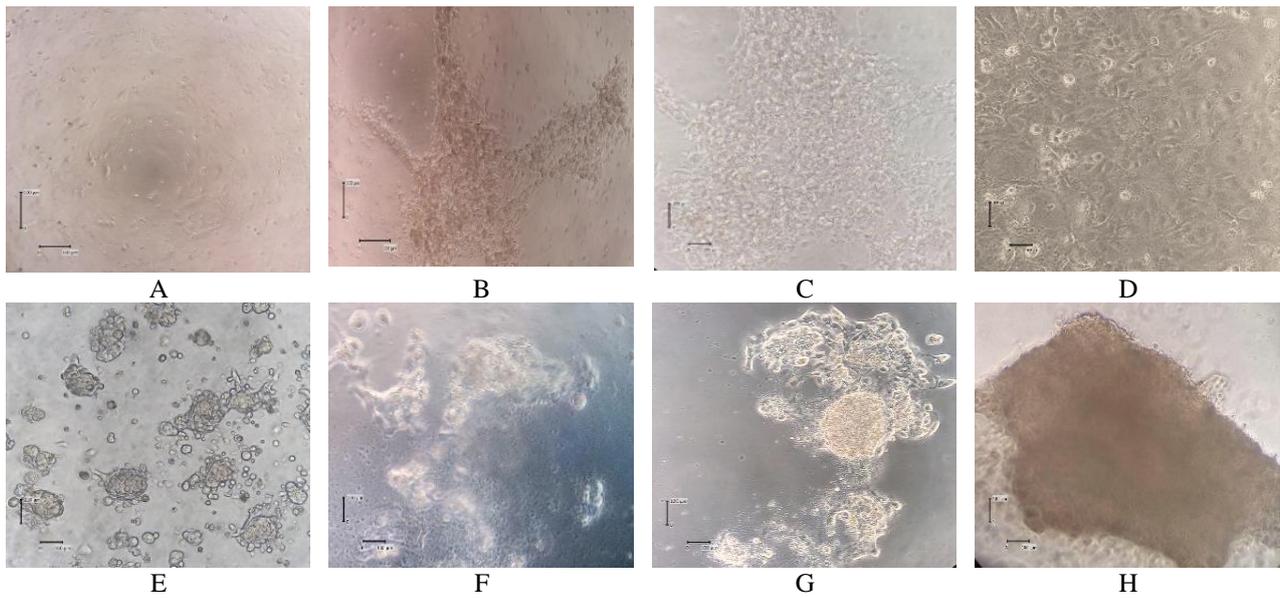
Figure 2. Gradual cellular morphology changes occur in 2D co-culture as shown in A–C. Initially, from 2D co-culture day 1, LX-2 cells appear as attached cells in a single layer, while CD34⁺ UCB SCs appear as small, round cells dispersed in motion or unattached to the well (A). After the second day in 2D co-culture, the single-layer LX-2 cells started to retract to the center of the well, thus forming a micromass (B). On day 3, a larger micromass is formed in 2D co-culture (C). This is called spheroid formation. Compared with 2D monoculture of LX-2 on day 3, spheroid formation is absent. LX-2 cells in 2D culture remain as single-layer cells attached to the well (D). In 3D co-culture, gradual morphology changes occur as shown in E–G. From 3D co-culture day 1, cell aggregates started to form and dispersed in the hanging drop (E). After day 2, 3D co-culture showed spheroid formation (F), which increased in size on day 3 (G). Compared with the 3D hanging drop of LX-2, the formation of larger spheroids was observed on day 3 (H). Magnification 200x
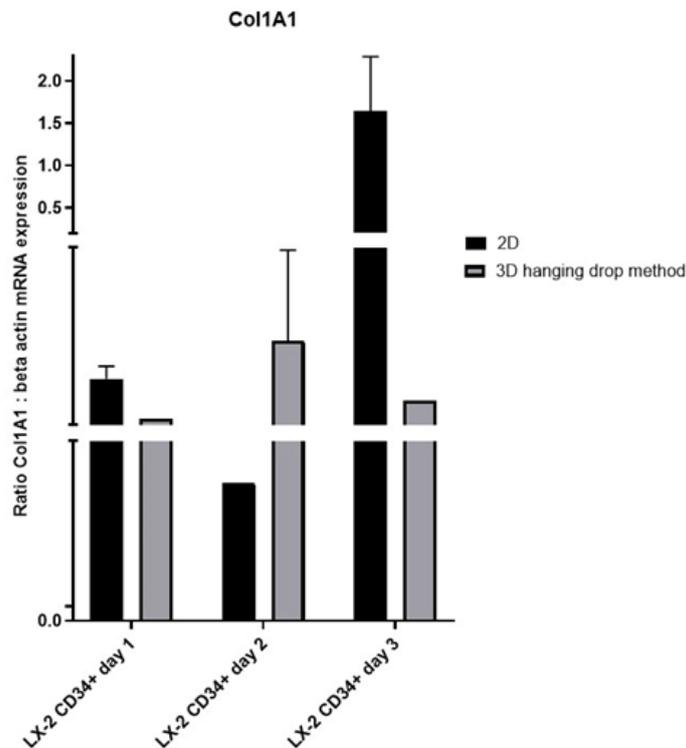

Figure 3. Normalized level of mRNA collagen 1A1 expression in 2D and 3D co-cultures of LX-2 and CD34⁺ UCB SCs. The ratio is normalized to LX-2 cell monoculture. Each bar represents the mean of triplicate replication of experiments. The error bar represents the standard deviation
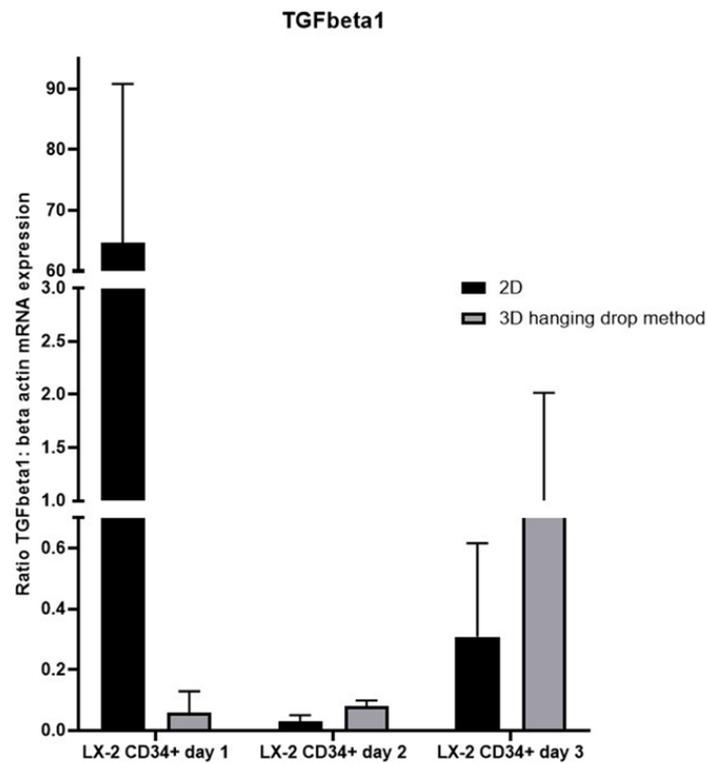
Figure 4. Normalized level of mRNA TGFbeta expression in 2D and 3D co-cultures of LX-2 and CD34$^+$ UCB SCs. The ratio is normalized to LX-2 cell monoculture. Each bar represents the median of triplicate replication of experiments. The maximum value is displayed as the upper line
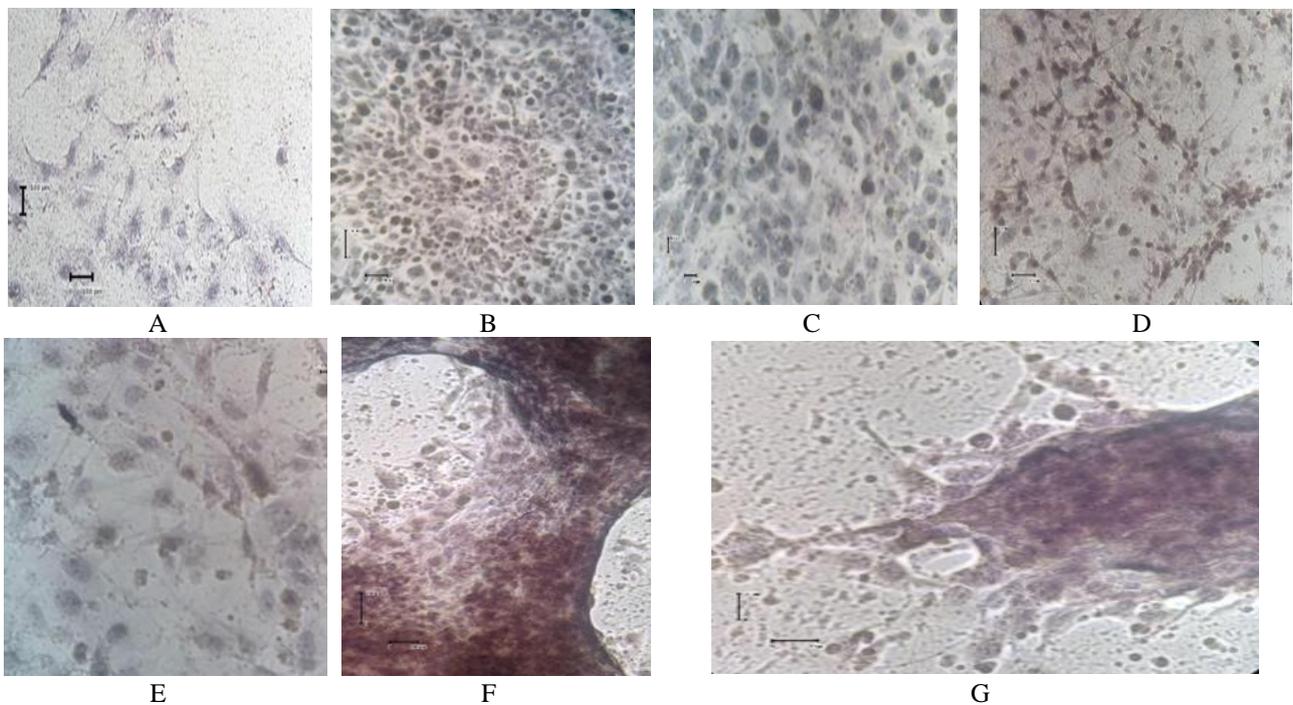

Figure 5. Immunocytochemistry of tenascin-C (A) Negative control for tenascin-C, magnification 200x (B–C) Monoculture LX2, magnification 200x and 400x (D-E) monoculture LX2 in mix medium (DMEM + RPMI), magnification 200x and 400x. (F-G) 2D co-culture of CD34+ UCB SCs and LX2, magnification 200x and 400x. Black bar indicates 10 µM

Tenascin-C expression in 2D co-culture and spheroid formation. Immunocytochemistry of tenascin-C from the 2D monoculture of LX-2 cells and 2D co-culture of CD34⁺ UCB SCs and LX-2 cells showed areas of dark brown chromogen substrate, which indicated immunoreactivity to tenascin-C (Figure 5). Immunoreactivity to tenascin-C (tenascin-C expression) is considered positive when the brown chromogen substrate (DAB) is deposited in the extracellular space or cell membrane. In Figure 4C and 4E, some of the cells showed brown chromogen substrates in the nucleus of the cells. This observation could have been due to nonspecific binding of the tenascin-C antibody. In Figure 4F and 4G, the area of the dark brown substrate was diffuse throughout the entire spheroid.

Immunocytochemistry of tenascin-C from the 3D co-culture of CD34⁺ UCB SCs and LX-2 cells was not established. The sample for immunohistochemistry of tenascin-C was scarce and difficult to handle. Despite the effort to cytospin, smear, and perform the drop method and cytoblock during the preparation of histology specimens, the 3D samples were lost during the subsequent liquid change or antibody incubations. This challenge became an obstacle in 3D co-culture tenascin-C analysis.

Discussion

Potential anti-fibrotic targets have been identified; however, effective clinical therapies are still lacking.[17] Therefore, it is important to develop novel strategies to suppress hepatic stellate cell activation for the treatment of fibrotic hepatic diseases.[18,19] CD34⁺ UCB SCs are a rich source for hematopoietic SCs and EPCs for use in stem-cell therapy. The purity of CD34⁺ UCB SCs isolated by magnetic separation in this study was 80%. This result is comparable to recent CD34⁺ isolation reports.[20] Several reasons for using CD34⁺ UCB SCs are the following: (i) their less invasive procurement compared to bone marrow biopsy; (ii) their higher proliferative capacity; (iii) their lower HLA expression; and (iv) their higher capacity for differentiation into hepatocytes compared with bone marrow hematopoietic SCs.[21,22]

The direct interaction of UCB SCs to LX-2 cells occurred on day 1 and was followed by indirect interaction of the LX-2 and UCB-SC secretome on days 2 and 3 of co-culture. Data from this study that supported the indirect interaction of LX-2 and UCB SCs include the absence of UCB-SC morphology after day 2 of co-culture and spheroid formation differences in the co-culture compared with monoculture. The difference in spheroid formation on day 3 in 2D co-culture vs. monolayer in monoculture demonstrated an indirect effect of CD34⁺ UCB SCs on LX-2. Differences in the size of spheroid formation between 3D coculture vs. large spheroid size in monoculture on day 3 also showed an indirect effect of CD34⁺ UCB SCs. The disappearance of CD34⁺ UCB-SC morphology after day 2 in co-culture demonstrated that the stem cells were no longer viable. The secretome of CD34⁺ UCB SCs remained in the vicinity of the LX-2 and altered the phenotype of LX-2 into activated LX-2 (myofibroblasts).

The difference in spheroid formation between 2D and 3D co-culture compared with monoculture control raises further questions as to the composition of ECM protein, specifically Col1A1 (collagen type 1A1). Liver fibrosis is marked by the deposition of Col1A1 from activated LX-2 in the co-culture. This study showed the highest peak Col1A1 expression on day 2 for 3D co-culture, while 2D co-culture showed the lowest peak Col1A1 expression, on day 2. Overall, the Col1A1 expression of 3D co-culture from day 1 to day 3 remained below the control (LX-2 monoculture 3D). This result correlates with the formation of smaller spheroids than the control. Lower Col1A1 deposition from activated LX-2 leads to a lower level of fibrosis. This means that in 3D co-culture, direct and indirect interaction of CD34⁺ UCB SCs and LX-2 demonstrated inhibition of liver fibrosis in vitro. In contrast, Col1A1 expression in 2D co-culture on day 3 showed the highest expression: higher than the control (LX-2 monoculture 2D). This result correlates more with spheroid formation than with the monolayer morphology of the control. Higher Col1A1 deposition from activated LX-2 yields a higher fibrosis level. This means that in 2D co-culture, direct and indirect interaction of CD34⁺ UCB SCs and LX-2 showed the promotion of liver fibrosis in vitro. Inhibition of in vitro liver fibrosis is shown by a reversal of hepatic stellate-cell activity from an active to a quiescent state, which was indicated by a decrease in COL1A1 expression.[23–25] Our 3D co-culture result is in line with the previous study, which demonstrated inhibition of in vitro liver fibrosis.

Our result of in vitro liver fibrosis inhibition in the 3D co-culture could be due to the CD34⁺ UCB-SC secretome. The content of the secretomes is EVs (extracellular vesicles), cytokines, and growth factors. EVs are small membrane vesicles released by almost all cell types that contribute to cell-mediated biological effects in the form of RNA (miRNA, non-coding[nc]-RNA, long non-coding [lnc]-RNA), lipid, or proteins.[26,27] Inactivation of LX-2 could be caused by the release of exosome-enriched Twist1 and miR214/199-5a clusters, thus reducing CCN2 expression.[28] Proteomics analysis of UCB secretome revealed TGF-β as one of the signaling proteins identified in the secretome.[29]

The TGF-β signaling pathway plays a key role in liver fibrosis and carcinogenesis.[3] This study showed that in 2D co-culture, TGF-β expression on day 1 was higher by a range of 46 to 83 fold control and decreased by a range of 101 to 300 fold control on day 2. On day 3, TGF-β expression increased by a range of two to 30 fold control in 2D co-culture. Our 3D co-culture result showed a different trend, with lower TGF-β expression compared with control on day 1 and day 2. However, on day 3, the maximum TGF-β expression exceeded the control by 60%. The results of this study demonstrate that a direct interaction between CD34^{+} UCB SCs and LX-2 is essential for the attenuation of TGF-β signaling, except for the result from 2D co-culture day 1. Loss of TGF-β attenuation occurs on day 3 in both 2D and 3D co-culture results due to the absence of CD34^{+} UCB SCs in co-culture after day 2. This result is in line with the results of previous studies on the co-culture of SCs and LX-2 cells.[30,31] The two studies demonstrated inhibition of LX-2 cell activity by attenuation of TGF-β signaling. However, this present study used CD34^{+} UCB SCs, while the aforementioned studies used bone marrow mesenchymal SCs. An in vivo study by Nakamura *et al.* reported that transplantation of CD34^{+} in rats with liver cirrhosis decreased TGF-β signaling and COL1A1 expression.[32,33] The potential for ligand-receptor binding between CD34^{+} UCB SCs and LX-2 to have caused attenuation in TGF-β signaling has not been identified to date. On day 3, the increase in TGF-β expression is due to the TGF-β from the secretome of CD34^{+} UCB SCs.

TGF-β functions as paracrine factor for vasculogenic mimicry in the HCC microenvironment. Vasculogenic mimicry is a special vascular structure for highly aggressive cancer.[34] Tenascin-C is an upregulated metastasis gene in 3D culture of high metastatic HCC spheroids.[35] Tenascin-C is highly expressed in cancer stroma (extracellular microenvironment). It plays a role in modulating the cancer cell microenvironment, thereby favoring metastasis.[36] Tenascin-C expression was observed in 2D co-culture of CD34^{+} UCB SCs and LX-2 in this present study. Tenascin-C plays an important role in the activation of hepatic stellate cells by mediating the interaction between TGF-β and α9β1 integrin. Previous study demonstrated an interaction that increased collagen type 1 production and hepatic stellate cell migration.[37]

The limitations of this study include challenges in the establishment of an immunocytochemistry protocol for tenascin-C and statistically insignificant differences between 2D and 3D co-culture. The lack of statistical difference between 2D and 3D co-culture results in this study restricts interpretation to one based on trends in the data. Future directions of this study include liver organoid as an integrated 3D liver

microenvironment for further investigation of hepatocytes-to-non-parenchymal liver cells and liver cells-to-ECM interactions during liver tissue changes, i.e., liver fibrogenesis and carcinogenesis.

Conclusion

Interaction between LX-2 and CD34^{+} UCB SCs in 3D co-culture inhibits in vitro liver fibrosis. Viable CD34^{+} UCB SCs are essential for attenuation of TGF-β signaling in LX-2.

Funding

Conflict of Interest Statement

The authors have no relevant affiliations or financial involvement with any organization with the subject matter or materials discussed in the manuscript.

References

1. Singal AG, Lampertico P, Nahon P. Epidemiology and surveillance for hepatocellular carcinoma: New trends. *J Hepatol.* 2020;72:250–61.
2. Kalinich M, Bhan I, Kwan TT, Miyamoto DT, Javaid S, LiCausi JA, *et al.* An RNA-based signature enables high specificity detection of circulating tumor cells in hepatocellular carcinoma. *Proc Natl Acad Sci USA.* 2017;114:1123–8.
3. Gianelli G, Villa E, Lahn M. Transforming growth factor-β as a therapeutic target in hepatocellular carcinoma. *Cancer Res.* 2014;74:1890–4.
4. Antarianto RD, Septiana WL, Jusuf AA, Barasila AC, Pawitan JA, Fasha I. Comparison of 2D and 3D co-culture with hanging drop method to produce a more clinically relevant microenvironment. *eJKI.* 2017;5:121–6.
5. Caicedo-Carvajal CE, Liu Q, Goy A, Pecora A, Suh KS. Three-dimensional cell culture models for biomarker discoveries and cancer research. *Transl Med.* 2012;S1:005.
6. Breslin S, O'Driscoll L. Three-dimensional cell culture: The missing link in drug discovery. *Drug Discov Today.* 2013;18:240–9.
7. Xu L, Hui AY, Albanis E, Arthur MJ, O'Byrne SM, Blaner WS, *et al.* Human hepatic stellate cell lines, LX-1 and LX-2: New tools for analysis of hepatic fibrosis. *Gut.* 2005;54:142–51.
8. Weiskirchen R, Weimer J, Meurer SK, Kron A, Seipel B, Vater I, *et al.* Genetic characteristics of the human hepatic stellate cell line LX-2. *PLoS One.* 2013;8:e75692.
9. Lin N, Chen Z, Lu Y, Li Y, Hu K, Xu R. Role of activated hepatic stellate cells in proliferation and metastasis of hepatocellular carcinoma. *Hepatol Res.* 2015;45:326–36.
10. Yin Z, Dong C, Jiang K, Xu Z, Li R, Guo K, *et al.*

Heterogeneity of cancer-associated fibroblasts and roles in the progression, prognosis, and therapy of hepatocellular carcinoma. *J Hematol Oncol*. 2019;12:101–9.

11. Li Z, Wu W, Zhao C, Zhao C, Zhang X, Yang Z, *et al*. CCN1/Cyr61 enhances the function of hepatic stellate cells in promoting the progression of hepatocellular carcinoma. *Int J Mol Med*. 2018; 41:1518–28.

12. Zekri ARN, Salama H, Medhat E, Musa S, Abdel-Halem H, Ahmed OS, *et al*. The impact of repeated autologous infusion of haematopoietic stem cells in patients with liver insufficiency. *J Stem Cell Res Ther*. 2015;6:118.

13. Meiliana A, Wijaya A. Application of umbilical cord Stem cells in regenerative medicine. *Indones Biomed J*. 2014;6:115–22.

14. Abdel Aziz MT, EL Asmar MF, Mostafa S, Salama H, Atta HM, Mahfouz S, *et al*. Reversal of hepatic fibrosis by human CD34+ stem/progenitor cell transplantation in rats. *Int J Stem Cells*. 2010;3:161–74.

15. Ilic D, Miere C, Lazic E. Umbilical cord blood stem cells: Clinical trials in non-hematological disorders. *Br Med Bull*. 2012;102:43–57.

16. Liu Z, Chen M, Zhao R, Huang Y, Liu F, Li B, *et al*. CAF-induced placental growth factor facilitates neoangiogenesis in hepatocellular carcinoma. *Acta Biochim Biophys Sin*. 2020;52:18–25.

17. Trautwein C, Friedman SL, Schupan D, Pinzani M. Hepatic fibrosis: from concept to treatment. *J Hepatol*. 2015;62:S15–24.

18. Soura S, Vives J. Extracellular vesicles: Squeezing every drop of regenerative potential of umbilical cord blood. *Metabolism*. 2019;95:102–4.

19. El Fiky BA, Elkhatib GZ, Eldahsan T. Hepatoprotective effects of umbilical cord blood stem cells against liver fibrosis in vivo. *AAMJ*. 2015;13:152–9.

20. Mata MF, Hernandez D, Rologi E, Grandolfo D, Hassan E, Hua P, *et al*. A modified CD34+ hematopoietic stem and progenitor cell isolation strategy from cryopreserved human umbilical cord blood. *Transfusion*. 2019;59:3560–9.

21. Roura S, Poujal JM, Gálvez-montón C, Bayes-Genis A. The role and potential of umbilical cord blood in an era of new therapies: A review. *Stem Cell Res Ther*. 2015;6:123.

22. Gabr H, Zayed R, El-zayat AR. Comparison between different cord blood stem cell populations in efficiency of transdifferentiation into hepatic lineage. *Ann Intl Interdisciplin Conf*. 2013;1:762–9.

23. Kisseleva T, Cong M, Paik Y, Scholten D, Jiang C, Benner C, *et al*. Myofibroblasts revert to an inactive phenotype during regression of liver fibrosis. *Proc Natl Acad Sci USA*. 2012;109:9448–53.

24. Liu X, Xu J, Brenner DA, Kisseleva T. Reversibility of liver fibrosis and inactivation of fibrogenic myofibroblasts. *Curr Pathobiol Rep*. 2013;1:209–14.

25. Mallat A, Lotersztajn S. Reversion of hepatic stellate cell to a quiescent phenotype: From myth to reality? *J Hepatol*. 2013;59:383–6.

26. Dong L, Pu Y, Chen X, Qi X, Zhang L, Xu L, *et al*. hUCMSC-extracellular vesicles downregulated hepatic stellate cell activation and reduced liver injury in S. japonicum-infected mice. *Stem Cell Res Ther*. 2020;11:21.

27. Yang J, Li C, Zhang L, Wang X. Extracellular vesicles as carriers of non coding RNA in liver diseases. *Front Pharmacol*. 2018;19:415.

28. Chen L, Brenner DA, Kisseleva T. Combatting fibrosis: exosome-based therapies in the regression of liver fibrosis. *Hepatol Commun*. 2019;3:180–92.

29. Sane MS, Tang H, Misra N, Pu X, Malara S, Jones CD, *et al*. Characterization of an umbilical cord blood sourced product suitable for allogeneic applications. *Regen Med*. 2019;14:769–89.

30. Zhang L-T, Fang X-Q, Chen Q-F, Chen H, Xiao P, Peng X-B, *et al*. Bone marrow-derived mesenchymal stem cells inhibit the proliferation of hepatic stellate cells by inhibiting the transforming growth factor β pathway. *Mol Med Rep*. 2015;2:7227–32.

31. Jang YO, Jun BG, Baik SK, Kim MY, Kwon SO. Inhibition of hepatic stellate cells by bone marrow-derived mesenchymal stem cells in hepatic fibrosis. *Clin Mol Hepatol*. 2015;21:141–9.

32. Nakamura T, Koga H, Iwamoto H, Tsutsumi V, Imamura Y, Naitou M, *et al*. Ex vivo expansion of circulating CD34(+) cells enhances the regenerative effect on rat liver cirrhosis. *Mol Ther Methods Clin Dev*. 2016;3:16025.

33. Sayyed HG, Osama A, Idriss NK, Sabry D, Abdelrhim AS, Bakry R. Comparison of the therapeutic effectiveness of human CD34 + and rat bone marrow mesenchymal stem cells on improvement of experimental liver fibrosis in Wistar rats. *Int J Physiol Pathophysiol Pharmacol*. 2016;8:128–39.

34. Yin Z, Jiang K, Li R, Dong C, Wang L. Multipotent mesenchymal stromal cells play critical roles in hepatocellular carcinoma initiation, progression and therapy. *Mol Cancer*. 2018;17:178.

35. Chen R, Dong Y, Xie X, Chen J, Gao D, Liu Y, Ren Z, Cui J. Screening candidate metastasis-associated genes in three-dimensional HCC spheroids with different metastasis potential. *Int J Clin Exp Pathol*. 2014;7:2527–35.

36. Midwood KS, Hussenet T, Langlois B, Orend G. Advances in tenascin-C biology. *Cell Mol Life Sci*. 2011;68:3175–99.

37. Ma J-C, Huang X, Shen Y-W, Zheng C, Su Q-H, Xu J-K, Zhao J. Tenascin-C promotes migration of hepatic stellate cells and production of type I collagen. *Biosci Biotechnol Biochem*. 2016;80:1470–7.